

Luminescent Gold(I) and Copper(I) Phosphane Complexes Containing the 4-Nitrophenylthiolate Ligand: Observation of $\pi \rightarrow \pi^*$ Charge-Transfer Emission

Cheng-Hui Li,^[a] Steven Chi Fai Kui,^[b] Iona Hiu Tung Sham,^[b] Stephen Sin-Yin Chui,^[b] and Chi-Ming Che^{*[a,b]}

Keywords: Gold / Copper / Phosphane / S ligands / Phosphorescence

Gold(I) and copper(I) phosphane complexes containing the 4-nitrophenylthiolate ligand, namely [(PCy₃)Au(SC₆H₄NO₂-4)] (**1**) (PCy₃ = tricyclohexylphosphane), [Au₂(μ -dcpm)(SC₆H₄NO₂-4)₂] (**2**) [dcpm = bis(dicyclohexylphosphanyl)methane], [Au₂(μ -dppm)(SC₆H₄NO₂-4)₂] (**3**) [dppm = bis(diphenylphosphanyl)methane], and [(μ -SC₆H₄NO₂-4)₂(μ -SC₆H₄NO₂-4)₂(CuPPh₃)₄] (**4**), were prepared and characterized by X-ray crystal analysis. All of these complexes show an intense absorption band with λ_{max} at 396–409 nm attributed to the intraligand (IL) $\pi(\text{S}) \rightarrow \pi^*(\text{C}_6\text{H}_4\text{NO}_2-4)$ charge-

transfer transition. The assignment is supported by the results of DFT and TDDFT calculations on the model complexes [PH₃Au(SC₆H₄NO₂-4)] and [(μ -SC₆H₄NO₂-4)₂(μ -SC₆H₄NO₂-4)₂(CuPPh₃)₄]. The emissions of solid samples and glassy solutions (methanol/ethanol, 1:4, v/v) of **1–4** at 77 K are assigned to the [$\pi(\text{S}) \rightarrow \pi^*(\text{C}_6\text{H}_4\text{NO}_2-4)$] charge-transfer excited state. Metallophilic interactions are not observed in both solid state and solutions of complexes **1–3**.

(© Wiley-VCH Verlag GmbH & Co. KGaA, 69451 Weinheim, Germany, 2008)

Introduction

Metal complexes with a d¹⁰ configuration, in particular those containing phosphane and/or thiolate ligands, exhibit interesting photophysical and photochemical properties.^[1,2] It is well documented that metallophilic interaction has a significant effect on the emission properties of this class of complexes.^[3,4] The emission from the metal-centred ³[5d σ^* 6p σ] excited state of binuclear gold(I) complexes with bridging phosphane ligands usually occurs in the UV region.^[5] If the counterion or solvent molecule is in the vicinity of the Au^I ion, an exciplex is readily formed and this leads to a red-shift in emission energy.^[5,6] A similar phenomenon has also been found for silver(I) and copper(I) phosphane complexes.^[3,4,7] For d¹⁰ metal phosphane complexes containing thiolate ligands, the thiolate to gold(I) charge-transfer excited state has often been proposed to account for their photoluminescence.^[8–10] In this work, we have prepared several d¹⁰ metal complexes which exhibit emissive $\pi \rightarrow \pi^*$ IL (intraligand) charge-transfer excited states. By utilizing the “donor–acceptor” type *p*-NO₂-C₆H₄SH ligand, we have obtained [(PCy₃)Au(SC₆H₄NO₂-4)] (**1**), [Au₂(μ -dcpm)(SC₆H₄NO₂-4)₂] (**2**), [Au₂(μ -dppm)(SC₆H₄NO₂-4)₂] (**3**), and [(μ -SC₆H₄NO₂-4)₂(μ -

SC₆H₄NO₂-4)₂(CuPPh₃)₄] (**4**). Complexes **1–4** represent examples of d¹⁰-metal thiolate complexes of which both the fluorescence and phosphorescence from intraligand $\pi \rightarrow \pi^*$ charge-transfer excited states could be observed.^[11–13]

Results and Discussion

Synthesis and Characterizations

Complexes **1–3** were prepared via the reaction of [(PCy₃)AuCl], [Au₂(μ -dcpm)Cl₂], or [Au₂(μ -dppm)Cl₂] with the 4-nitrophenylthiolate ligand in the presence of KOH. Complex **4** was prepared by reacting [Cu(SC₆H₄NO₂-4)]_∞ with triphenylphosphane. All four complexes are stable in both solid state and CH₂Cl₂ solutions, and have been characterized by elemental analyses, ¹H NMR and ³¹P NMR spectroscopy, and X-ray diffraction studies. The ³¹P NMR spectrum of **4** shows two signals, whereas that of **1–3** shows a single signal in each case. This is consistent with the fact that the phosphorus atoms in **4** are in different coordination environments as revealed by its crystal structure.

Crystal Structures

The crystal data of **1–4** are listed in Table 5,^[14] while selected bond lengths and angles of **1–3** and **4** are listed in Tables 1 and 2, respectively. Complex **1** has a slightly bent geometry [P(1)–Au(1)–S(1) 171.64(5)°, Figure 1] in which the nitro group is almost coplanar with the thiophenyl moiety. The Au–P distance [2.268(2) Å] of **1** is slightly longer

[a] Coordination Chemistry Institute and the State Key Laboratory of Coordination Chemistry, Nanjing University, Nanjing 210093, PR China

[b] Department of Chemistry and the HKU-CAS Joint Laboratory on New Materials, The University of Hong Kong, Pokfulam Road, Hong Kong SAR, PR China
E-mail: cmche@hku.hk

Supporting information for this article is available on the WWW under <http://www.eurjic.org/> or from the author.

than that for other literature-reported gold(I) phosphane complexes containing thiolate ligands (2.239–2.257 Å).^[15] This is presumably due to the inductive effect of the nitro group. On the other hand, the Au–S distance of 2.297(2) Å in **1** is comparable to that in [(PPh₃)Au{SC₆H₄(*m*-Cl)}] [2.292(2) Å]^[15] and falls within the range of typical values (2.291–2.314 Å) reported for gold(I) phosphane thiolate complexes.^[15] Neighbouring molecules of **1** are arranged in a tilted head-to-tail fashion at a dihedral angle of 22.7°. The tilting could be related to the intermolecular hydrogen bonding [O(2)⋯H(11B) 2.498 Å] and short C⋯H contacts [C(21)⋯H(9A) 2.868 Å and C(24)⋯H(10B) 2.745 Å].

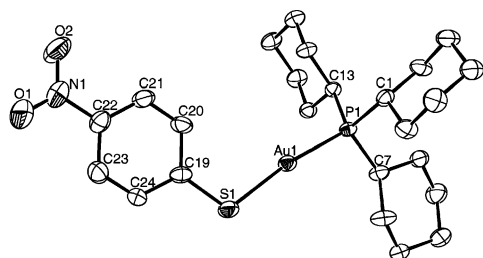


Figure 1. Molecular structure of **1** with thermal ellipsoids at 30% probability. Hydrogen atoms are omitted for clarity.

The coordination geometry of the Au atom in **2** slightly deviates from linearity [P(1)–Au(1)–S(1) 173.34(7)°, Figure 2]. Each molecule of **2** has a C₂ symmetry with a crystallographic twofold rotation axis that passes through the carbon atom [C(1)] of the methylene group and lies on the P–CH₂–P plane of the dcpm ligand. The Au–P distance [2.264(2) Å] of **2** is comparable to that of **1** [2.268(2) Å] while its Au–S distance [2.303(2) Å] is slightly longer [2.297(2) Å for **1**]. The two P–Au–S moieties bridged by the diphosphane ligand are directed away from each other, presumably due to the chelating effect of the dcpm ligand and the dipolar repulsion between the two 4-nitrophenylthiolate ligands (Figure 2). The planes of the two 4-nitrophenyl moieties in **2** are almost parallel as in the case of **1**. Interestingly, there is weak hydrogen bonding between O(1) of the 4-NO₂C₆H₄S ligand and C–H moieties of the dcpm ligand [O(1)⋯H(1A) 2.456 Å, O(1)⋯H(9B) 2.676 Å, and O(1)⋯H(7B) 2.692 Å] in addition to that involving O(2) [O(2)⋯H(9A) 2.719 Å].

X-ray crystal structure analysis revealed that **3** adopts an *anti* conformation in the solid state. Figure 3 depicts the molecular structure of **3**, in which there are two chemically equivalent but crystallographically inequivalent AuSC₆H₄NO₂–4 moieties bridged by a dppm ligand. The *anti* conformation is imposed by the sterically bulky phenyl groups of the dppm ligand, and is stabilized by intermolecular hydrogen bonding [O(1)⋯H(37B) 2.334 Å, O(4)⋯H(37A) 2.426 Å, and O(2)⋯H(5) 2.654 Å], short O⋯C contact [between a NO₂ group and the C–H group on the methylene, O(1)⋯C(37) 3.219 Å], and weak C–H interactions [C(12)⋯H(29) 2.830 Å and C(1)⋯H(11) 2.900 Å]. It is worth noting that for [Au{P-(CH₂)_{*n*}-P}X₂] (X = halide or

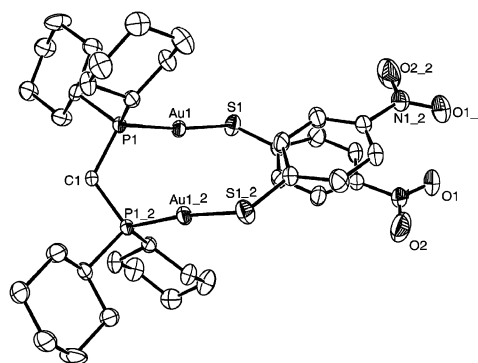


Figure 2. Molecular structure of **2** with thermal ellipsoids at 30% probability. Hydrogen atoms are omitted for clarity.

thiolate; where *n* = 1), the *anti* conformation is less commonly encountered as Au^I⋯Au^I interaction would favour a *syn* conformation.^[16,17,18] Since the bridging diphosphane ligand in **3** has only one –CH₂– unit, the dipolar interaction between the two 4-nitrophenylthiolate ligands accounts for the *anti* conformation.

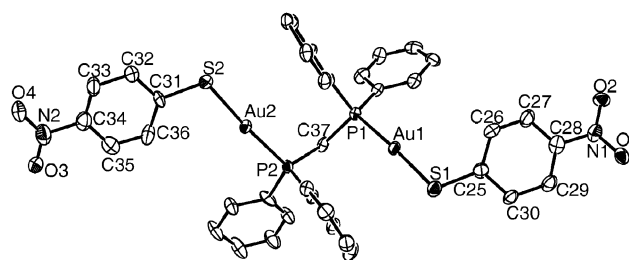


Figure 3. Molecular structure of **3** with thermal ellipsoids at 30% probability. Hydrogen atoms are omitted for clarity.

Au^I⋯Au^I interaction has not been observed in the solid state of **1–3**. The shortest Au^I⋯Au^I distance in **2** is 4.522 Å (Table 1). This distance is significantly longer than the sum of van der Waals radii (3.7 Å) for two gold atoms. The absence of aurophilic interactions is probably a consequence of steric hindrance of the phosphane ligands and dipolar repulsive interaction of the 4-nitrophenylthiolate ligands.

Table 1. Selected bond lengths [Å] and angles [°] for **1–3**.

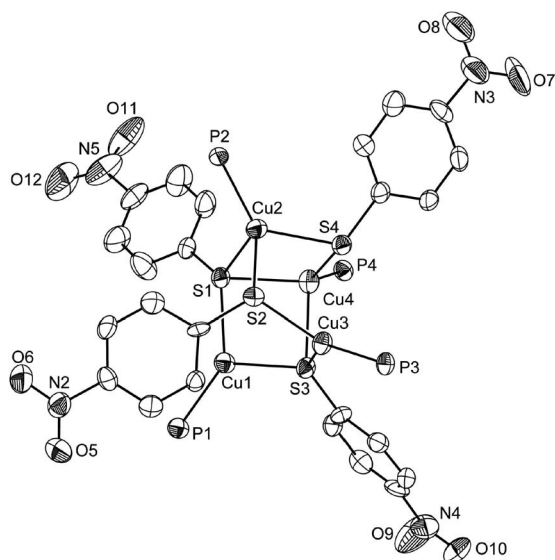
	1	2	3
Au(1)–P(1)	2.268(2)	2.264(2)	2.257(2)
Au(1)–S(1)	2.297(2)	2.303(2)	2.289(3)
Au(2)–P(2)	–	–	2.267(2)
Au(2)–S(2)	–	–	2.284(3)
Au ^I ⋯Au ^I (intramolecular)	–	4.522	5.387
Au ^I ⋯Au ^I (intermolecular)	7.690	8.425	7.414
P(1)–Au(1)–S(1)	171.64(5)	173.34(7)	175.2(1)
P(2)–Au(2)–S(2)	–	–	175.4(7)

The structure of **4** is depicted in Figure 4. Unlike [(μ₃-SPh)₂(μ-SPh)₂(CuPPh₃)₄] with a “step” structure,^[19] it has a Cu₄S₄ core in a distorted “open” cubane-like framework. Most of the Cu⋯S distances (2.254–2.552 Å) fall within the

range of values reported for steric bulky polynuclear copper(I) thiolate complexes with phosphane ligands.^[19–21] However, the Cu(1)–S(2) [3.957(5) Å] and Cu(3)–S(4) [2.964(4) Å] distances are too long to be considered as a bond and some of the angles significantly deviate from 90° (77–121°) revealing that **4** would be more appropriately described to have a distorted “open” cubane structure (Table 2). Such distortion might be caused by steric repulsion between triphenylphosphane and *p*-NO₂C₆H₄S ligands. In the crystal structure of **4**, there are two S···H contacts [S(2)···H(60) 2.955 Å] formed between two neighbouring molecules in each unit cell.^[22] The crystal structure also reveals the presence of other intermolecular interactions including (i) hydrogen bonding which involve the O atoms of NO₂ groups and the phenyl C–H of phosphane ligands

(O···H distance of 2.459–2.683 Å) or those of neighbouring *p*-NO₂C₆H₄S ligands (2.441–2.698 Å), (ii) O···C contacts (3.109–3.214 Å), (iii) C···H interactions between aryl C atoms of the *p*-NO₂C₆H₄S ligand and H atoms of the triphenylphosphane ligand (2.741–2.825 Å). Of particular interest is that one of the NO₂ groups is involved in a bifurcated H-bond network [N(2)–O(6)···H(4)–C(4) 2.459 Å and N(2)–O(6)···H(55)–C(68) 2.521 Å]. Both the copper and sulfur atoms in **4** individually have two coordination modes. Two of the copper atoms are triply coordinated [μ_3 ; Cu(1) and Cu(3); denoted by Cu_{trig}] and the other two copper atoms are in a tetrahedral environment [μ_4 ; Cu(2) and Cu(4); denoted by Cu_{tet}]. For the sulfur atoms, S(2) and S(4) are doubly bridging (μ_2) while S(1) and S(3) are triply bridging (μ_3). The Cu–S distances range with the coordination modes of the copper and sulfur atoms: Cu_{tet}–(μ_3 -S) (average: 2.468 Å) > Cu_{tet}–(μ_2 -S) (2.348 Å) > Cu_{trig}–(μ_3 -S) (2.268 Å) and Cu_{trig}–(μ_2 -S) (2.287 Å). The six Cu–Cu distances, in the range of 3.02–4.12 Å, are greater than the sum of van der Waals radii of 2.80 Å, thus there is no Cu^I···Cu^I interaction in **4**.

(a)



(b)

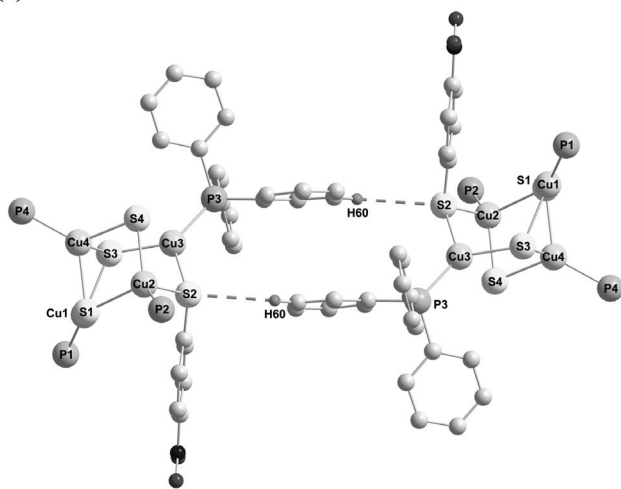


Figure 4. (a) Molecular structure of **4** with thermal ellipsoids at 30% probability. Hydrogen atoms and the phenyl groups on the triphenylphosphane ligands are omitted for clarity. (b) Interaction between two molecules of **4** in the unit cell viewed along the *b*-axis.

Table 2. Selected bond lengths [Å] and angles [°] for **4**.

Cu(1)–S(1)	2.271(2)	Cu(2)–S(1)	2.467(2)
Cu(1)···S(2)	3.957(4)	Cu(2)–S(2)	2.395(3)
Cu(1)–S(3)	2.279(2)	Cu(2)–S(4)	2.332(3)
Cu(1)–P(1)	2.184(2)	Cu(2)–P(2)	2.243(3)
Cu(3)–S(2)	2.287(3)	Cu(4)–S(1)	2.385(3)
Cu(3)–S(3)	2.254(2)	Cu(4)–S(3)	2.552(3)
Cu(3)···S(4)	2.964(4)	Cu(4)–S(4)	2.318(2)
Cu(3)–P(3)	2.195(3)	Cu(4)–P(4)	2.223(3)
S(2)···H(60)	2.955(4)	Cu(2)···Cu(4)	3.0248(2)
P(1)–Cu(1)–S(1)	140.36(9)	P(1)–Cu(1)–S(3)	124.0(1)
S(1)–Cu(1)–S(3)	95.65(9)	S(1)–Cu(4)–S(3)	86.07(8)
P(2)–Cu(2)–S(4)	129.33(9)	P(2)–Cu(2)–S(2)	116.89(9)
P(2)–Cu(2)–Cu(4)	143.78(8)	P(2)–Cu(2)–S(1)	118.87(9)
S(2)–Cu(2)–S(1)	95.0(1)	S(2)–Cu(2)–Cu(4)	99.17(7)
P(3)–Cu(3)–S(3)	129.8(1)	P(3)–Cu(3)–S(2)	124.9(1)
S(3)–Cu(3)–S(2)	105.05(9)	S(3)–Cu(4)–Cu(2)	94.06(7)
P(4)–Cu(4)–S(4)	122.51(9)	P(4)–Cu(4)–S(1)	123.67(9)
P(4)–Cu(4)–S(3)	122.0(1)	P(4)–Cu(4)–Cu(2)	143.93(8)
S(4)–Cu(2)–S(2)	89.62(9)	S(4)–Cu(2)–S(1)	98.98(9)
S(4)–Cu(4)–S(1)	101.78(9)	S(4)–Cu(4)–S(3)	91.44(9)
Cu(1)–S(1)–Cu(4)	84.73(9)	Cu(1)–S(1)–Cu(2)	121.0(1)
Cu(4)–S(1)–Cu(2)	77.10(7)	Cu(3)–S(3)–Cu(1)	117.5(1)
Cu(3)–S(3)–Cu(4)	98.25(9)	Cu(1)–S(3)–Cu(4)	80.81(8)
Cu(3)–S(2)–Cu(2)	101.7(1)	Cu(4)–S(4)–Cu(2)	81.15(8)

Absorption Spectroscopy

The spectroscopic data of **1–4** are summarized in Table 3. The electronic absorption spectra of **1–4** in CH₂Cl₂ solutions at 298 K show an intense band with λ_{max} at 396–409 nm and a shoulder at 254–259 nm (Figure 5). Complexes **3** and **4** show additional shoulders at 277–280 nm (Table 3). Assignment of the absorption bands are based on comparison with the spectroscopic data of [Au(PR₃)Cl] complexes, and on the coordination number of copper atoms as well as coordination mode of the thiolate ligands.^[9,16,18,23] The shoulders at 254–259 nm are attributed

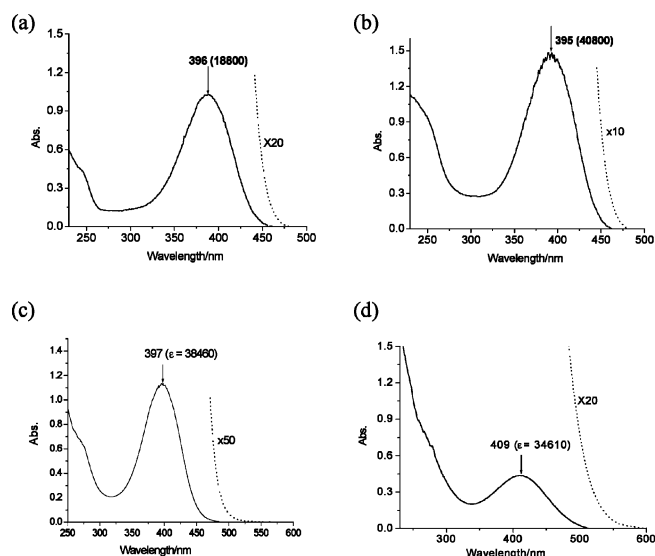


Figure 5. Absorption spectra of (a) **1**, (b) **2**, (c) **3**, and (d) **4** in CH₂Cl₂ solutions at 298 K.

Table 3. Absorption and photophysical data for **1–4**.

<i>T</i> [K]	Medium	λ_{abs} [nm] ^[a] ϵ [dm ³ mol ⁻¹ cm ⁻¹] ^[b]	λ_{em} [nm] ^[c] τ [μ s] ^[d]
298	CH ₂ Cl ₂	254 (sh, 7120), 396 (18800), 465 (25)	nonemissive
	solid		nonemissive
	77 solid		450, 470 (<0.08) 531 (3.6), 564
77	MeOH/ EtOH, 1:4		452, 471 (<0.08), 533 (3.8), 564
298	CH ₂ Cl ₂	254 (sh, 25030), 399 (40800), 470 (30)	nonemissive
	solid		nonemissive
	77 solid		475 (sh, <0.08) 546, 577 (4.3)
77	MeOH/ EtOH, 1:4		468 (<0.08), 546 (4.4), 576
298	CH ₂ Cl ₂	257 (sh, 23730), 277 (20980), 397 (34860), 490 (45)	nonemissive
	solid		nonemissive
	77 solid		443 (<0.08), 608 (2.5)
77	MeOH/ EtOH, 1:4		459 (<0.08), 547 (2.6)
298	CH ₂ Cl ₂	259 (sh, 62110), 280 (sh, 48715), 409 (34610), 530 (70)	nonemissive
	solid		631 (0.2)
	77 solid		485 (<0.08), 634 (3.4)
77	MeOH/ EtOH, 1:4		469 (<0.08), 523 (4.0), 554

[a] Absorption maximum at 5×10^{-5} M. [b] Molar extinction coefficient. [c] Emission maximum. [d] Emission lifetime.

to $\pi(\text{phenyl}) \rightarrow \pi^*(\text{phenyl})$ transitions since the 4-nitrophenylthiolate ligand exhibits a similar absorption shoulder. Complexes **3** and **4** absorb more strongly than **1** and **2** in the spectral region 277–280 nm, presumably this is caused by the intraligand transition of the phenyl groups of the phosphane ligands. The intense band with λ_{max} at 396–409 nm is red-shifted from the gold complexes (**1–3**, 396–399 nm) to the copper complex (**4**, 409 nm, Table 3), indicating that the energy of this transition is affected by the metal ion. An ethanolic solution of KSC₆H₄NO₂-4 exhibits an intense absorption at $\lambda_{\text{max}} = 420$ nm, while that of the free ligand is at 356 nm. On the basis of these findings, we assign the absorption at $\lambda_{\text{max}} = 396$ –409 nm to the $[\pi(\text{S}) \rightarrow \pi^*(\text{C}_6\text{H}_4\text{NO}_2-4)]$ intraligand charge-transfer transition and the shift in λ_{max} values could be accounted for by the perturbation in electronic charge on the thiolate S atom by H⁺, Cu^I, or Au^I.

The solvent effect on the absorption spectra of **1–4** has been studied (Table 4 and the absorption spectra of **1–4** in various solvents are given in the Supporting Information).

Table 4. Solvent effect on the absorption spectra of **1–4**.

Complex	Solvent ^[a]	λ_{abs} [nm] ϵ [dm ³ mol ⁻¹ cm ⁻¹]
1	CH ₂ Cl ₂	396 (16810)
	MeOH (96%) + CH ₂ Cl ₂ (4%)	385 (12890)
	MeCN (96%) + CH ₂ Cl ₂ (4%)	391 (13330)
	(CH ₃) ₂ CO (96%) + CH ₂ Cl ₂ (4%)	392 (18820)
	THF	397 (20470)
	DMF	399 (18780)
	DMSO	402 (19700)
	C ₆ H ₆ (96%) + CH ₂ Cl ₂ (4%)	393 (19080)
	EA (96%) + CH ₂ Cl ₂ (4%)	394 (21700)
	2	CH ₂ Cl ₂
MeOH (96%) + CH ₂ Cl ₂ (4%)		390 (28300)
MeCN (96%) + CH ₂ Cl ₂ (4%)		396 (40060)
(CH ₃) ₂ CO (96%) + CH ₂ Cl ₂ (4%)		400 (34990)
THF		399 (33340)
DMF		405 (33050)
DMSO		409 (38130)
C ₆ H ₆ (96%) + CH ₂ Cl ₂ (4%)		393 (22320)
EA (96%) + CH ₂ Cl ₂ (4%)		393 (21530)
3		CH ₂ Cl ₂
	MeOH (96%) + CH ₂ Cl ₂ (4%)	392 (30100)
	MeCN (96%) + CH ₂ Cl ₂ (4%)	394 (34610)
	(CH ₃) ₂ CO (96%) + CH ₂ Cl ₂ (4%)	398 (37350)
	THF	399 (44200)
	DMF	407 (35420)
	DMSO	407 (32800)
	C ₆ H ₆ (96%) + CH ₂ Cl ₂ (4%)	394 (33700)
	EA (96%) + CH ₂ Cl ₂ (4%)	393 (38600)
	4	CH ₂ Cl ₂
MeOH (96%) + CH ₂ Cl ₂ (4%)		408 (22900)
MeCN (96%) + CH ₂ Cl ₂ (4%)		434 (18190)
(CH ₃) ₂ CO (96%) + CH ₂ Cl ₂ (4%)		404 (11160)
THF		401 (20400)
DMF		440 (26980)
DMSO		445 (18800)
C ₆ H ₆ (96%) + CH ₂ Cl ₂ (4%)		401 (39180)
EA (96%) + CH ₂ Cl ₂ (4%)		403 (31260)

[a] EA = ethyl acetate.

The solvent effect on the absorption λ_{max} of **1–3** is minimal; for example, the $[\pi(\text{S}) \rightarrow \pi^*(\text{C}_6\text{H}_4\text{NO}_2-4)]$ transition of **1** spans only a narrow range of 385–402 nm when the solvent changes from methanol to dimethyl sulfoxide. In contrast, the absorption λ_{max} of **4** undergoes a larger shift upon changing the solvent from CH_2Cl_2 (406 nm) to CH_3CN (434 nm), DMF (440 nm), and DMSO (445 nm).

Emission Spectroscopy

The photophysical data of **1–4** are summarized in Table 3. Complexes **1–4** are nonemissive in CH_2Cl_2 solutions. At 298 K, a solid sample of **4** exhibits an intense emission with λ_{max} at 631 nm while **1–3** are nonemissive under the same conditions. Upon excitation at 360 nm at 77 K, solid samples of **1–4** individually show dual emissions with λ_{max} at 443–485 and 564–634 nm (Table 3). For each complex, the lower energy emission is more intense than the higher energy one. The higher energy emission, in each case, has a lifetime in the nanosecond time regime while the lifetimes of all the lower energy emissions are in the microsecond time regime; hence the emission with λ_{max} at 443–485 nm correspond to fluorescence while that at 564–634 nm is phosphorescence. The solid state emission of **1** is vibronically structured with peak maxima at 450, 470, 531, and 564 nm. The average vibronic spacing is 1023 cm^{-1} and could be assigned to $\nu(\text{C}=\text{C})$ stretching in the $\pi^*(\text{C}_6\text{H}_4\text{NO}_2-4)$ excited states.

Dual emissions have also been observed for **1–4** in glassy solutions (methanol/ethanol, 1:4, v/v) at 77 K (Figure 6). The emissions with λ_{max} at 452–469 nm are comparable in energy to the high energy solid-state emission of **1–4** recorded at 77 K. For **3** and **4**, their lower energy emission

λ_{max} are blue-shifted from 608 and 634 nm in the solid state to 547 and 523 nm in glassy solutions, respectively. This blue-shift in emission λ_{max} is not surprising since excited-state structural distortion is diminished in frozen glassy solutions. The excitation spectra (Figure 6) recorded for the emission of **1–4** in glassy solutions individually show a band with λ_{max} at 392–413 nm. On the basis of the similarity between the excitation spectra and the corresponding absorption spectra, in addition to the results of emission lifetime measurements, the lower energy emissions (λ_{max} at 523–634 nm, Table 3) of **1–4** in the solid state and glassy solutions at 77 K are assigned to the $^3[\pi(\text{S}) \rightarrow \pi^*(\text{C}_6\text{H}_4\text{NO}_2-4)]$ (intraligand charge-transfer) excited state.

The polarization ratios of the lower energy emissions of **1–4** were estimated using the following equation.

$$\text{Polarization ratio: } \frac{I_{\text{VV}} \cdot I_{\text{HH}}}{I_{\text{VH}} \cdot I_{\text{HV}}}$$

where I_{VV} is intensity with both polarizers at 0° ; I_{HH} is intensity with both polarizers at 90° ; I_{VH} is intensity with polarizers crossed (excitation: vertical; emission: horizontal); I_{HV} is intensity with polarizers crossed (excitation: horizontal; emission: vertical). The polarization ratios are: 0.74 for **1** at 533 nm; 1.07 for **2** at 546 nm; 0.99 for **3** at 547 nm; 1.09 for **4** at 523 nm.

Computational Results

DFT calculations on the model complexes $[(\text{PH}_3)\text{-Au}(\text{SC}_6\text{H}_4\text{NO}_2-4)]$ and $[(\mu_2\text{-SC}_6\text{H}_4\text{NO}_2-4)_2(\mu_3\text{-SC}_6\text{H}_4\text{NO}_2-4)_2(\text{CuPH}_3)_4]$ were performed. The mononuclear $[(\text{PH}_3)\text{-Au}(\text{SC}_6\text{H}_4\text{NO}_2-4)]$ was used to model **1–3** as there is no $\text{Au}^1 \cdots \text{Au}^1$ interaction found in their crystal structures. The complex $[(\mu_2\text{-SC}_6\text{H}_4\text{NO}_2-4)_2(\mu_3\text{-SC}_6\text{H}_4\text{NO}_2-4)_2(\text{CuPH}_3)_4]$ was used to model **4**. The geometries of the model complexes were fully optimized in their ground states without symmetry constraint. The quality of the optimized structures (Figure 7) was checked by comparing the results with the X-ray crystal structures of **1–4**. For $[(\text{PH}_3)\text{-Au}(\text{SC}_6\text{H}_4\text{NO}_2-4)]$, the calculated Au–S and Au–P distances are 2.354 and 2.333 Å, respectively, which are in good agreement with the experimental values (Au–S 2.29–2.32 Å, Au–P 2.26–2.28 Å for **1–3**). On the other hand, the calculated S–C (1.783 Å), N–C (1.466 Å), and N–O (1.236 Å) distances are slightly longer than the experimental values of 1.74–1.75, 1.39–1.50, and 1.20–1.27 Å found for **1–3**, respectively. The complex $[(\mu_2\text{-SC}_6\text{H}_4\text{NO}_2-4)_2(\mu_3\text{-SC}_6\text{H}_4\text{NO}_2-4)_2(\text{CuPH}_3)_4]$ has a distorted cubane structure as in **4**. The calculated Cu–P (2.195–2.228 Å) and Cu–S (2.267–2.466 Å) distances are also comparable to those of **4** (2.19–2.25 and 2.26–2.47 Å, respectively).

On the basis of the optimized structures of the model complexes depicted in Figure 7, TD-DFT calculations were performed to check the assignment of the absorption spectra. The calculated lowest energy dipole allowed transitions could be compared to the intense absorptions of **1–4** at $\lambda_{\text{max}} = 396\text{--}409 \text{ nm}$. The lowest energy absorption for $[(\text{PH}_3)\text{-Au}(\text{SC}_6\text{H}_4\text{NO}_2-4)]$ was calculated at 405 nm. This corre-

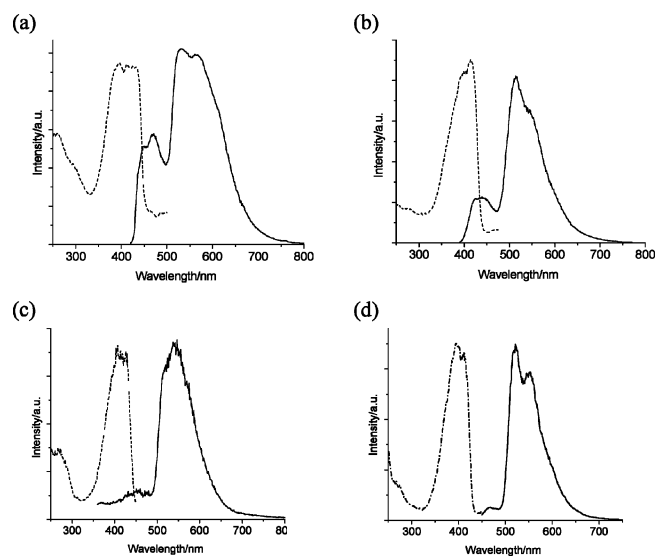


Figure 6. Excitation (dashed) and emission (solid) spectra of (a) **1**, (b) **2**, (c) **3**, and (d) **4** in glassy solutions (methanol/ethanol, 1:4, v/v) at 77 K.

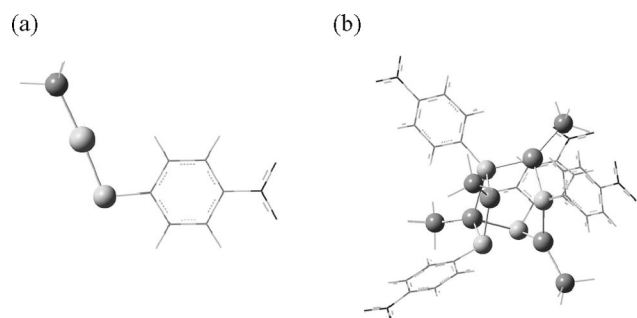


Figure 7. DFT-optimized geometries of (a) $[(\text{PH}_3)\text{Au}(\text{SC}_6\text{H}_4\text{NO}_2-4)]$ and (b) $[(\mu_2\text{-SC}_6\text{H}_4\text{NO}_2-4)_2(\mu_3\text{-SC}_6\text{H}_4\text{NO}_2-4)_2(\text{CuPH}_3)_4]$.

sponds to the transition from HOMO to LUMO. Population analysis revealed that the HOMO of $[(\text{PH}_3)\text{Au}(\text{SC}_6\text{H}_4\text{NO}_2-4)]$ is mainly of $\text{S}(p_\pi)$ orbital character (62.04% p_π orbital of the sulfur atom and 34.75% p_π orbital of the *p*-nitrophenyl moiety), while the LUMO is dominated by p_π orbitals of the *p*-nitrophenyl moiety (97.87%) as depicted in Figure 8.

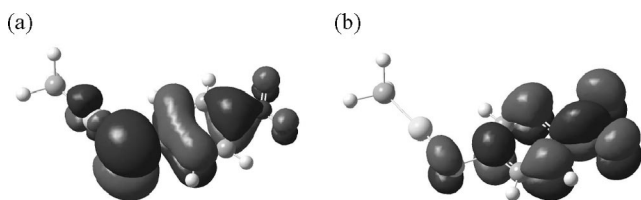


Figure 8. Representation of the (a) HOMO and (b) LUMO for $[(\text{PH}_3)\text{Au}(\text{SC}_6\text{H}_4\text{NO}_2-4)]$ involved in the lowest energy transition.

For $[(\mu_2\text{-SC}_6\text{H}_4\text{NO}_2-4)_2(\mu_3\text{-SC}_6\text{H}_4\text{NO}_2-4)_2(\text{CuPH}_3)_4]$, several electronic transitions at 397–415 nm have been calculated. These transitions involve electronic excitation from HOMO-1 and HOMO to several unoccupied molecular orbitals from LUMO to LUMO+3. The HOMO-1 and HOMO of $[(\mu_2\text{-SC}_6\text{H}_4\text{NO}_2-4)_2(\mu_3\text{-SC}_6\text{H}_4\text{NO}_2-4)_2(\text{CuPH}_3)_4]$ are mainly of $\text{S}(p_\pi)$ character (HOMO-1, 50.5% p_π orbital of the sulfur atom and 45.3% p_π orbital of the *p*-nitrophenyl moiety; HOMO, 50.69% p_π orbital of the sulfur atom and 45.12% p_π orbital of the *p*-nitrophenyl moiety), while the LUMO to LUMO+3 are localized on the p_π orbitals of the *p*-nitrophenyl groups (89.94%, 88.59%, 89.42%, and 87.13% for LUMO, LUMO+1, LUMO+2, and LUMO+3, respectively) as depicted in Figure 9. The metal ions of both $[(\text{PH}_3)\text{Au}(\text{SC}_6\text{H}_4\text{NO}_2-4)]$ and $[(\mu_2\text{-SC}_6\text{H}_4\text{NO}_2-4)_2(\mu_3\text{-SC}_6\text{H}_4\text{NO}_2-4)_2(\text{CuPH}_3)_4]$ have no more than 5% contribution to the molecular orbitals involved in the calculated electronic transitions at 397–415 nm. Therefore, the calculated electronic transitions at 405 nm in the cases of 1–3 and 397–415 nm in the case of 4 are assigned to the intraligand charge-transfer transition mainly from the π electrons (p_π) of the S atom to the π^* orbitals of the *p*-nitrophenyl moiety. The calculated transition energies are in good agreement with the experimental values, 396 nm for 1 and 409 nm for 4 (Table 3).

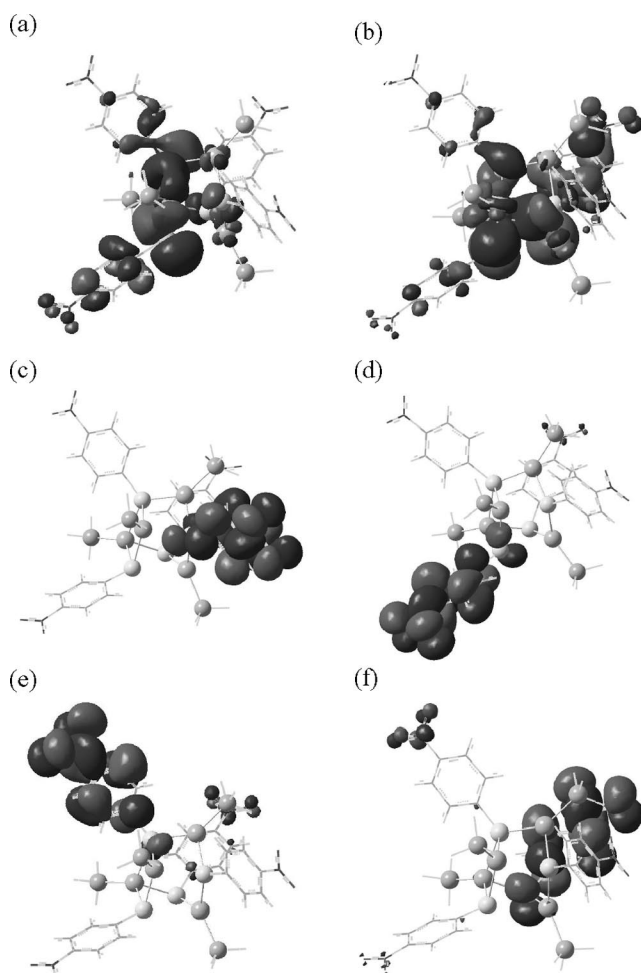


Figure 9. Representation of the (a) HOMO-1, (b) HOMO, (c) LUMO, (d) LUMO+1, (e) LUMO+2, and (f) LUMO+3 for $[(\mu_2\text{-SC}_6\text{H}_4\text{NO}_2-4)_2(\mu_3\text{-SC}_6\text{H}_4\text{NO}_2-4)_2(\text{CuPH}_3)_4]$ involved in the lowest energy transitions.

Concluding Remarks

A series of gold(I) and copper(I) phosphane complexes containing the 4-nitrophenylthiolate ligand have been synthesized and structurally characterized. No metal–metal interaction was found in the crystal structures of 1–4. Complexes 1–4 exhibit phosphorescence at 560–632 nm in addition to fluorescence at 440–485 nm. The intense absorption at 395–410 nm is assigned to the $\pi(\text{S}) \rightarrow \pi^*(\text{C}_6\text{H}_4\text{NO}_2-4)$ transition and the assignment is supported by the results of DFT and TD-DFT calculations. Accordingly, the phosphorescence of 1–4 is assigned to the ${}^3[\pi(\text{S}) \rightarrow \pi^*(\text{C}_6\text{H}_4\text{NO}_2-4)]$ excited state.

Experimental Section

Reagents and Instrumentation: ${}^1\text{H}$ NMR and ${}^{31}\text{P}$ NMR spectra were recorded with Bruker AMX-300/400 spectrophotometers at 298 K in CDCl_3 . Elemental (C, H, and N) analyses were performed with a Perkin–Elmer 240C analyzer. UV/Vis absorption spectra were obtained with a Perkin–Elmer Lambda 19 UV/Vis spectrophotometer. Emission spectra were recorded with a SPEX Flu-

rolog-3 spectrophotometer. Low-temperature (77 K) emission spectra were recorded with the sample in glassy [methanol/ethanol (4:1, v/v)] solution or in solid form placed in a quartz tube (with a 5 mm diameter) in a Dewar immersed with liquid nitrogen. The emission spectra were corrected for the efficiency of the monochromator and photomultiplier and stability of the xenon lamp. Emission lifetime measurements were carried out with a Quanta Ray DCR-3 pulsed Nd:YAG laser system (pulse output 355 nm, 8 ns).

All reactions were conducted under a nitrogen atmosphere at room temperature using standard Schlenk techniques. 4-Nitrothiophenol, PCy₃ (tricyclohexylphosphane), dppm [bis(diphenylphosphanyl)methane], and dcpm [bis(dicyclohexylphosphanyl)methane] were obtained from commercial sources. [(PCy₃)AuCl], [Au₂(μ-dppm)Cl₂], and [Au₂(μ-dcpm)Cl₂] were prepared using the procedure described for the synthesis of [Au(PR₃)X].^[24] [Cu(SC₆H₄NO₂-4)]_∞ was prepared using the method described for [Cu(SC₆H₅)]_∞.^[25]

[PCy₃)Au(SC₆H₄NO₂-4)] (1): A solution of KSC₆H₄NO₂-4, prepared in situ by reacting HSC₆H₄NO₂-4 (0.155 g, 1.00 mmol) and KOH (1 molar equiv.) in MeOH (10 mL), was added dropwise to a CH₂Cl₂ solution (20 mL) of [(PCy₃)AuCl] (0.247 g, 0.500 mmol). The mixture was stirred overnight before the solvent was removed. The residue was extracted using dichloromethane and precipitation was induced by adding diethyl ether (20 mL). The solid was washed with diethyl ether and dried in vacuo. Recrystallization of the crude product was carried out via vapour diffusion of diethyl ether into dichloromethane solution. Yield 0.52 g, 82%. C₂₄H₃₇AuNO₂PS (631.54): calcd. C 45.64, H 5.91, N 2.22; found C 45.44, H 5.74, N 2.50. ¹H NMR (300 MHz, CDCl₃): δ = 7.93 (d, ³J = 8.4 Hz, 2 H, aryl H *ortho* to S), 7.62 (d, ³J = 8.4 Hz, 2 H, aryl H *meta* to S), 2.13–1.23 (m, 33 H, Cy) ppm. ³¹P{¹H} NMR (400 MHz, CDCl₃): δ = 58.73 (s) ppm.

[Au₂(μ-dcpm)(SC₆H₄NO₂-4)₂] (2): A solution of HSC₆H₄NO₂ (0.124 g, 0.600 mmol) and KOH (0.045 g, 0.60 mmol) in methanol (20 mL) was added to a dichloromethane solution (20 mL) of [Au₂(dcpm)Cl₂] (0.349 g, 0.400 mmol). The mixture was stirred overnight before the solvent was removed. The residue was extracted with dichloromethane and precipitation was induced by

adding diethyl ether (20 mL). The solid was washed with diethyl ether and dried in vacuo. The crude product was recrystallized by vapour diffusion of diethyl ether into dichloromethane solution. Yield 0.38 g, 86%. C₃₇H₅₄Au₂N₂O₄P₂S₂ (1110.82): calcd. C 40.01, H 4.90, N 2.52; found C 39.78, H 4.85, N 2.76. ¹H NMR (300 MHz, CDCl₃): δ = 7.91 (d, ³J = 8.2 Hz, 4 H, aryl H *ortho* to S), 7.60 (d, ³J = 8.1 Hz, 2 H, aryl H *meta* to S), 2.23–1.29 (m, 44 H, dcpm; 2 H, -PCH₂P-) ppm. ³¹P{¹H} NMR (400 MHz, CDCl₃): δ = 50.25 (s) ppm.

[Au₂(μ-dppm)(SC₆H₄NO₂-4)₂] (3): Complex 3 was prepared in a similar manner to 2, except that dppm was used instead of dcpm. Yield 75%. C₃₇H₃₀Au₂N₂O₄P₂S₂ (1086.62): calcd. C 40.90, H 2.78, N 2.58; found C 40.92, H 2.90, N 3.09. ¹H NMR (300 MHz, CDCl₃): δ = 3.73 (m, 2 H, -PCH₂P-), 7.27–7.99 (m, 8 H, C₆H₄; 20 H, dppm) ppm. ³¹P{¹H} NMR (400 MHz, CDCl₃): δ = 31.53 (s) ppm.

[(μ₂-SC₆H₄NO₂-4)₂(μ₃-SC₆H₄NO₂-4)₂(CuPPh₃)₄] (4): PPh₃ (0.215 g, 0.820 mmol) was added to a suspension of [Cu(SC₆H₄NO₂-4)]_∞ (0.179 g, 0.820 mmol) in dichloromethane (20 mL). The mixture was stirred for 5 h and a clear red solution was obtained. Removal of the solvent gave a red solid which was washed with diethyl ether. Yield 0.32 g, 79%. C₉₆H₇₆Cu₄N₄O₈P₄S₄ (1919.89): calcd. C 60.05, H 3.99, N 2.92; found C 60.01, H 3.91, N 2.98. ¹H NMR (300 MHz, CDCl₃): δ = 7.19–7.69 (m, 16 H, C₆H₄; 60 H, PPh₃) ppm. ³¹P{¹H} NMR (400 MHz, CDCl₃): δ = 31.39 (s), -1.21 (s) ppm.

X-ray Crystallography: The diffraction data of 1–4 (Table 5) were obtained with a Siemens (Bruker) SMART CCD diffractometer using graphite-monochromated Mo-K_α radiation (λ = 0.71073 Å). Cell parameters were retrieved using the SMART software and refined using SAINT on all observed reflections.^[26] Data were collected using the following strategy: 606 frames of 0.3° in ω with φ = 0°, 435 frames of 0.3° in ω with φ = 90°, and 235 frames of 0.3° in ω with φ = 180°. An additional 50 frames of 0.3° in ω with φ = 0° were collected to allow for decay correction. The raw intensity data sets were reduced using SAINT and corrected for Lorentz and polarization effects. Absorption corrections were applied using

Table 5. Crystal data for 1–4.

	1	2	3	4
Formula	C ₂₄ H ₃₇ AuNO ₂ PS	C ₃₇ H ₅₄ Au ₂ N ₂ O ₄ P ₂ S ₂	C ₃₇ H ₃₀ Au ₂ N ₂ O ₄ P ₂ S ₂	C ₉₆ H ₇₆ Cu ₄ N ₄ O ₈ P ₄ S ₄
M _r [g mol ⁻¹]	631.54	1110.82	1086.62	1919.89
Crystal system	monoclinic	monoclinic	triclinic	triclinic
Space group	P2 ₁ /c	C2/c	P1	P1
a [Å]	9.429(3)	18.006(9)	10.876(2)	14.130(3)
b [Å]	24.699(7)	12.942(9)	11.102(2)	14.858(3)
c [Å]	10.609(3)	17.117(8)	15.990(3)	22.812(5)
α [°]	90.00	90.00	72.58(3)	88.78(3)
β [°]	99.241(5)	95.00(5)	82.19(3)	86.90(3)
γ [°]	90.00	90.00	86.23(3)	63.99(3)
Z	4	4	2	2
V [Å ³]	2438.8(1)	3974(4)	1824.4(7)	4297.7(15)
D _{calc} [g cm ⁻³]	1.720	1.857	1.978	1.484
M [mm ⁻¹]	6.204	7.601	8.276	1.209
F(000)	1256	2168	1036	1968
2θ _{max} [°]	56.20	52.90	50.14	50.80
No. of reflections (unique)	13214 (5271)	10693 (4034)	6801 (6426)	15979 (15312)
Parameters	271	222	442	1081
GoF	0.973	0.905	1.07	0.923
R ₁ ^[a] [I > 2σ(I)]	0.074	0.066	0.050	0.251
wR ₂ ^[b] [I > 2σ(I)]	0.123	0.075	0.130	0.169
Residual peak/hole [e Å ⁻³]	1.485/−2.715	1.534/−1.107	0.892/−2.398	0.679/−0.411

[a] R₁ = Σ||F_o| − |F_c||/Σ|F_o|. [b] wR₂ = [Σw(|F_o| − |F_c||)²/Σw|F_o|²]^{1/2}.

SADABS supplied by Bruker.^[27] The structures were solved by direct methods using the program SHELXL-97 and refinement of F^2 by full-matrix least-squares procedures was carried out with SHELXTL software.^[28] All non-hydrogen atoms were anisotropically refined. The hydrogen atoms were located theoretically and not refined.^[14]

Computational Details: Calculations on the electronic ground and excited states of the metal complexes were carried out using B3LYP density functional theory. B3LYP corresponds to the combination of Becke's three-parameter exchange functional (B3) with the Lee–Yang–Parr for the correlation functional (LYP). Quasi-relativistic pseudo-potentials proposed by Wadt and Hay^[29–30] with 19 valence electrons and the LANL2DZ basis sets for Au, Cu, P, S, C, and H were adopted. Two additional f-type functions are supplemented for Au ($\alpha_f = 0.2, 1.19$), Cu ($\alpha_f = 0.24, 3.70$)^[31] and one d-type function is added to S ($\alpha_d = 0.421$), P ($\alpha_d = 0.34$), O ($\alpha_d = 1.154$), N ($\alpha_d = 0.864$), and P ($\alpha_d = 0.6$), respectively.^[32] The initial models were used from the crystal structure. To save computational resources, the phenyl and cyclohexyl groups were represented by hydrogen in all calculations of this work, as this has been validated by previous studies.^[6,33–34] The equilibrium ground-state geometries were computed using the B3LYP functional with the LanL2DZ basis set and fully optimized without symmetry constraints. At the correct ground-state geometry optimizations, time-dependent DFT (TDDFT) calculations using the B3LYP functional were performed to obtain the electronic transition energy of the model complexes. The solvent effect was simulated by using the polarizable continuum model (PCM), in which the solvent cavity is seen as a union of interlocking atomic spheres. All the calculations described here were carried out by using the Gaussian 03 package.^[35]

Supporting Information (see also the footnote on the first page of this article): Crystal structure of **1**, absorption and emission spectra of **1–4** in various media, absorption spectrum of the 4-nitrophenylthiolate ligand.

Acknowledgments

We gratefully acknowledge financial support by the National Natural Science Foundation of China, Research Grants Council - Joint Research Scheme (N_HKU 742/04).

- [1] P. C. Ford, E. Cariati, J. Bourassa, *Chem. Rev.* **1999**, *99*, 3625–3647.
- [2] V. W.-W. Yam, K. K.-W. Lo, *Chem. Soc. Rev.* **1999**, *28*, 323–334.
- [3] C.-M. Che, S.-W. Lai, *Coord. Chem. Rev.* **2005**, *249*, 1296–1309.
- [4] D. L. Phillips, C.-M. Che, K. H. Leung, Z. Mao, M.-C. Tse, *Coord. Chem. Rev.* **2005**, *249*, 1476–1490.
- [5] W.-F. Fu, K.-C. Chan, V. M. Miskowski, C.-M. Che, *Angew. Chem. Int. Ed.* **1999**, *38*, 2783–2785.
- [6] H.-X. Zhang, C.-M. Che, *Chem. Eur. J.* **2001**, *7*, 4887–4893.
- [7] Z. Mao, H.-Y. Chao, Z. Hui, C.-M. Che, W.-F. Fu, K.-K. Cheung, N. Zhu, *Chem. Eur. J.* **2003**, *9*, 2885–2894.
- [8] P. J. Costa, M. J. Calhorda, *Inorg. Chim. Acta* **2006**, *359*, 3617–3624.
- [9] C.-K. Li, X.-X. Lu, K. M.-C. Wong, C.-L. Chan, N. Zhu, V. W.-W. Yam, *Inorg. Chem.* **2004**, *43*, 7421–7430.
- [10] V. W.-W. Yam, C.-K. Li, C.-L. Chan, *Angew. Chem. Int. Ed. Engl.* **1998**, *37*, 2857–2859.
- [11] C.-M. Che, H.-Y. Chao, V. M. Miskowski, Y. Li, K.-K. Cheung, *J. Am. Chem. Soc.* **2001**, *123*, 4985–4991.

- [12] H.-Y. Chao, W. Lu, Y. Li, M. C. W. Chan, C.-M. Che, K.-K. Cheung, N. Zhu, *J. Am. Chem. Soc.* **2002**, *124*, 14696–14706.
- [13] W. Lu, H.-F. Xiang, N. Zhu, C.-M. Che, *Organometallics* **2002**, *21*, 2343–2346.
- [14] CCDC-651974 (for **1**), -651975 (for **2**), -651976 (for **3**), -651977 (for **4**) contain the supplementary crystallographic data for this paper. These data can be obtained free of charge from The Cambridge Crystallographic Data Centre via www.ccdc.cam.ac.uk/data_request/cif.
- [15] J. M. Forward, D. Bohmann, J. P. Fackler Jr, R. J. Staples, *Inorg. Chem.* **1995**, *34*, 6330–6336.
- [16] S.-Y. Ho, E. C.-C. Cheng, E. R. T. Tiekink, V. W.-W. Yam, *Inorg. Chem.* **2006**, *45*, 8165–8174.
- [17] A. Maspero, I. Kani, A. A. Mohamed, M. A. Omary, R. J. Staples, J. P. Fackler Jr, *Inorg. Chem.* **2003**, *42*, 5311–5319.
- [18] R. Narayanaswamy, M. A. Young, E. Parkhurst, M. Ouellette, M. E. Kerr, D. M. Ho, R. C. Elder, A. E. Bruce, M. R. M. Bruce, *Inorg. Chem.* **1993**, *32*, 2506–2517.
- [19] I. G. Dance, M. L. Scudder, L. J. Fitzpatrick, *Inorg. Chem.* **1985**, *24*, 2547–2550.
- [20] H. Xu, J. H. K. Yip, *Inorg. Chem.* **2003**, *42*, 4492–4494.
- [21] T. C. Deivaraj, G. X. Lai, J. J. Vittal, *Inorg. Chem.* **2000**, *39*, 1028–1034.
- [22] S. B. Novaković, B. Fraisse, G. A. Bogdanović, A. S. Bivé, *Cryst. Growth Des.* **2007**, *7*, 191–195.
- [23] M. M. Savas, W. R. Mason, *Inorg. Chem.* **1987**, *26*, 301–307.
- [24] A. K. Al-Sa'ady, C. A. McAuliffe, R. V. Parish, J. A. Sandbank, R. A. Potts, W. T. Schneider, *Inorg. Synth.* **1985**, *23*, 191–194.
- [25] I. G. Dance, P. J. Guernsey, A. D. Rae, M. L. Scudder, *Inorg. Chem.* **1983**, *22*, 2883–2887.
- [26] Siemens, *SAINTE*, v4 Software Reference Manual, Siemens Analytical X-ray Systems, Inc., Madison, WI, USA, **1996**.
- [27] G. M. Sheldrick, *SADABS*, Program for Empirical Absorption Correction of Area Detector Data, University of Göttingen, Göttingen, Germany, **1996**.
- [28] Siemens, *SHELXTL*, Version 5.1, Reference Manual, Siemens Analytical X-ray Systems, Inc., Madison, WI, USA, **1996**.
- [29] W. R. Wadt, P. J. Hay, *J. Chem. Phys.* **1985**, *82*, 284–298.
- [30] W. R. Wadt, P. J. Hay, *J. Chem. Phys.* **1985**, *82*, 299–310.
- [31] P. Pykkö, F. Mendizabal, *Inorg. Chem.* **1998**, *37*, 3018–3025.
- [32] S. Huzinaga, *Gaussian Basis Sets for Molecular Calculations*, Elsevier, Amsterdam, **1984**.
- [33] P. Pykkö, Y. Zhao, *Angew. Chem. Int. Ed. Engl.* **1991**, *30*, 604–605.
- [34] B.-H. Xia, H.-X. Zhang, C.-M. Che, K.-H. Leung, D. L. Phillips, N. Zhu, Z.-Y. Zhou, *J. Am. Chem. Soc.* **2003**, *125*, 10362–10374.
- [35] M. J. Frisch, G. W. Trucks, H. B. Schlegel, G. E. Scuseria, M. A. Robb, J. R. Cheeseman, V. G. Zakrzewski, J. A. Montgomery Jr, R. E. Stratmann, J. C. Burant, S. Dapprich, J. M. Millam, A. D. Daniels, K. N. Kudin, M. C. Strain, O. Farkas, J. Tomasi, V. Barone, M. Cossi, R. Cammi, B. Mennucci, C. Pomelli, C. Adamo, S. Clifford, J. Ochterski, G. A. Petersson, P. Y. Ayala, Q. Cui, K. Morokuma, D. K. Malick, A. D. Rabuck, K. Raghavachari, J. B. Foresman, J. Cioslowski, J. V. Ortiz, A. G. Baboul, B. B. Stefanov, G. Liu, A. Liashenko, P. Piskorz, I. Komaromi, R. Gomperts, R. L. Martin, D. J. Fox, T. Keith, M. A. Al-Laham, C. Y. Peng, A. Nanayakkara, M. Challacombe, P. M. W. Gill, B. Johnson, W. Chen, M. W. Wong, J. L. Andres, C. Gonzalez, M. Head-Gordon, E. S. Replogle, J. A. Pople, *Gaussian 03*, Revision B.05 (Gaussian 98, Revision A.9), Gaussian, Inc., Pittsburgh, PA, **2003**.

Received: June 29, 2007

Published Online: April 15, 2008